FRACTAL PRECISION MODELS OF LATHE-TYPE TURNING MACHINES

Irem Y. Tumer, R. S. Srinivasan, Kristin L. Wood, Ilene Busch-Vishniac
Department of Mechanical Engineering
The University of Texas
Austin, Texas

ABSTRACT

The primary objective of this research is to develop surface models of machining processes to simulate machined surface profiles and analyze their structure. In this paper, fractal analysis is used to discover and characterize the variational pattern of turned surfaces. This analysis provides a means of explicitly stating the precision of a machining process. The results are used to further test the validity of the concept of fractal dimensions at tolerance scales and to establish a relation between surface models, experimental surfaces, and fractals. Based on these results, a more complete model of turning is available to designers for choosing process and design parameters and for comparing the precision between competing machining processes.

INTRODUCTION

Objectives and Scope

Manufacturing methods are receiving more attention as a crucial technology for industrial competitiveness. It is insufficient to consider only the functional aspects of products. Instead, an understanding of manufacturing process capabilities and limitations must be developed to improve product quality. One approach to enable this understanding is the creation of more precise models of machining processes. Precision models are instrumental in characterizing machined surfaces, especially the relationship between the surface quality and the product function. Measures for conveying the precision of machining processes are design tolerances. Tolerances are the scale of interest since they provide a link between design information (desired product surfaces), and manufacturing information (actual surfaces produced by machining).

The crucial role of tolerances in design and manufacturing has been the motivation for numerous research efforts. A fractal-based tolerancing approach to analyzing surface structure has been proposed previously by Srinivasan and Wood [21, 22]. Fractal-based tolerancing techniques provide an index to the variational structure of a machined surface. This index will provide a means of choosing preferred machining processes, cutting parameters, and design parameters to be used for a part or assembly. This paper extends these ideas in an effort to apply the fractal-based analysis to a more comprehensive and realistic surface model of machining processes, namely turning.

In an effort to extend the work, simulation results based on a study of turning surface characteristics are presented. An extensive study of the mechanics of machining processes leads to the development of a comprehensive turning model, based on component and system dynamics. The study also uses the development of three-dimensional force relationships at the tool-workpiece contact area. Simulation of the turning model provides a basis for analyzing the structure of the machined surface by means of fractal-based methods.

In the following sections, the tolerance representation and fractal-based approach are discussed. A brief background on metal cutting, machining errors, and a review of literature on metal cutting models are presented next. A detailed presentation of the turning model then sets the foundation for the simulations. The simulation results are accompanied by a fractal analysis and compared to the previous results [21]. The paper concludes with an interpretation of the simulation results and a discussion of possible improvements of the model.

Tolerances in Machining Processes

The magnitude of tolerances is a major contributing factor of the cost and quality of a product. The present work is aimed at studying the surface characteristics and corresponding tolerance magnitudes of machined components based on the mechanics of metal removal. In metal cutting, a thin layer of metal, the chip, is removed by a wedge-shaped tool from a larger body, the workpiece [4]. Metal removal unavoidably generates irregular surface variations that depart from the ideal surface profile. By providing a tolerance specification prior to machining a part, the designer can account for this surface variation. Given the machining process and the cutting and design parameters, a tolerance zone can be predicted.

Research in the tolerance area has been pursued for many years. A brief summary of some of the major tolerancing techniques is presented here. For a comprehensive summary of tolerancing techniques, the reader is referred to Zhang and Huq [30]. The major areas of research in tolerancing methods are divided into three categories: tolerance chaining, geometric modeling, and statistical and probabilistic tolerancing.

When transforming stock material into components within the tolerance specifications of design representations, the feasibility of the process sequence is checked via a tolerance chain. The tolerance chain yields a set of linear algebraic expressions relating design dimensions to individual machining cuts. With the advent of computer-integrated manufacturing, tolerance chains can be assigned and analyzed computationally. Numerous computer-aided tolerance chain techniques have been developed. Bjorke [1] uses the concept of tolerance chaining in calculating tolerances, using an interactive computer program called Toltech.

The area of research in geometric modeling has been fragmented. There is currently a need to integrate the different theories and standardize these in a common approach [30]. Requicha [18] describes tolerances as being specified by designers, who should ensure that parts within tolerance specification are functionally equivalent and assemblable. Although geometric (solid) modeling is expected to become the primary source of geometric information in integrated design and production systems, geometrical modeling systems presently do not yet provide complete tolerancing facilities. Neither do they fully support automatic process planning or perform spatial reasoning required for assemblability analysis [30]. Currently, the theories are based on geometrical conformity and are not in accordance with the general tolerancing philosophy, which reflects the current industrial practice based on functional requirements [30].

Statistical and probabilistic methods in tolerancing, like Monte Carlo and Taguchi, currently only consider discrete tolerance evaluation of one-dimensional linear or nonlinear assemblies. The Monte Carlo method has been used to generate the parameters of the design function distribution. Taguchi's method uses the quality loss function concept and is based on an experimental design approach [30].

Most of the tolerancing methods in the literature concern size tolerances only, geometric tolerancing not yet having a unified and complete strategy. Due to the strong geometric basis of fractals, it is hypothesized that fractal-based tolerancing methods can represent geometric tolerances more effectively. As a result, the ongoing research program is aimed at determining a more structured method of assigning geometric tolerances according to the machining process used and the cutting and design parameters employed. To enable a prediction of the structure of the generated surface profile, it is proposed to model the machining processes and analyze the resulting surface profile. In this work, a turning process is considered in terms of the circularity tolerance of a cylindrical workpiece.

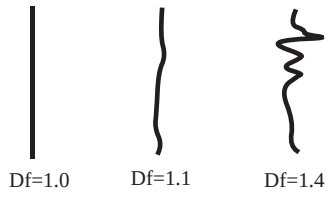

Figure 1: Illustration of the Fractal Dimension Concept.

Use of Fractal-Based Methods

Fractals have been proposed as a means of characterizing surface irregularities, and, originally, surfaces occurring in nature [13]. Mandelbrot's [13] fractal geometry provides both a description and a mathematical model for many complex forms in nature, such as coastlines, clouds, and mountains. These complex forms of nature possess a statistical self-similarity that can be quantified by a fractal dimension. While geometry in general concerns three-dimensional objects, the present paper deals with a special case, circularity tolerances related to surface profiles. The fractal dimension determines the relative degree of detail or irregularity of surfaces. Profiles with a larger fractal dimension appear more irregular [17]. For instance, an ideally smooth surface with no irregularity is assumed to have a fractal dimension of one, whereas a real profile may have a fractal dimension between one and two. Figure 1 shows characteristic fractal dimensions for three surface profiles. The higher the fractal dimension, the more irregular is the surface. For more details on fractals, the reader is referred to Mandelbrot [13] and Peitgen and Saupe [17].

Srinivasan and Wood [21] show that tolerance scales are fractal and suggest that fractal-based methods be used as a new approach to geometric tolerancing, based on the strong geometric basis of fractals. Fractals have been used in the literature to analyze surface finish [7, 11, 12]. A fractal-based parameter, the fractal dimension, is used to characterize the variational pattern of the microgeometry. Majumadar and Bhushnan [11] have studied the role of fractal geometry in roughness characterization of surfaces. In this study, roughness measurements of a variety of surfaces show surface profiles that can be linked mathematically to the

concepts of self-similarity and self-affinity. Since the fractal dimension is scale-invariant and linked to these concepts, they conclude the natural use of fractal geometry to characterize rough surfaces and to provide the geometric structure at all length scales. In a study by Majumdar and Tien [12], the fractal dimension is identified as an intrinsic property of a multiscale and random roughness structure. Roughness measurements on a variety of stainless steel surfaces and a textured magnetic thin-film rigid disk show that their spectra follow power laws within the length scales considered. They therefore suggest that the roughness structure can be characterized by fractal geometry. In a study by Church [7], it is shown that the roughness of many highly finished optical surfaces is more accurately described by fractal rather than conventional methods.

In comparison to the above references, this research focuses on tolerance-scale surface characteristics, as opposed to surface finish. Using the fractal-based methods developed in [21], it is possible to compute a fractal dimension from the simulated surface profile. The fractal-based methods use a box-counting algorithm to compute the fractal dimension. A fractal dimension characterizes the structure of a surface profile variation caused by internal and external machining errors, the machining parameters, and the machining process itself. Internal errors are surface deviations caused by the system components, their physical properties, their motion, and their interaction, whereas external errors are transmitted through the system foundations from external sources. By providing an index of the variational pattern of a machined surface profile, fractal dimensions may be assigned to particular machining processes and parameters. This will enable the designer to assign more accurate tolerances to the components to be machined.

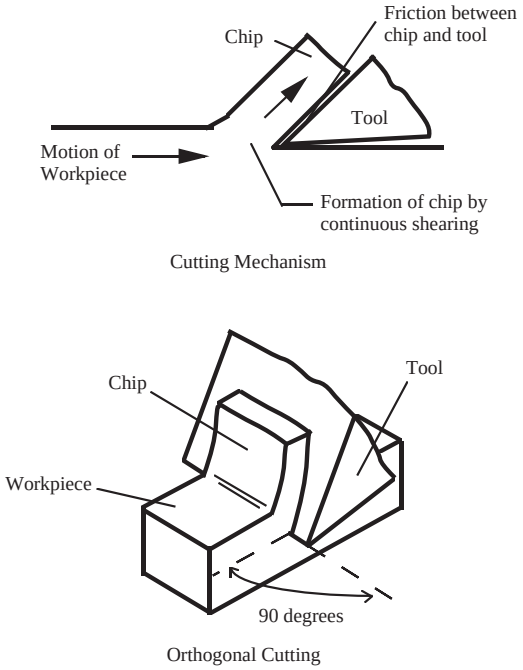

Figure 2: Basic Model of the Cutting Process.

BACKGROUND

Before developing the surface models of machining processes, an understanding of the metal cutting mechanism is essential. The following subsections give a brief review of the metal cutting process and machining errors, followed by a review of the literature on metal cutting models.

Metal Cutting

The cutting process is basically one of shearing the work material to form a chip, producing friction on the cutting-tool face as the chip is removed. This basic concept of the cutting process is illustrated in Figure 2. Metal-cutting operations use a wedge-shaped tool, which has a straight cutting edge, and is constrained to move relative to the workpiece in such a way that a layer of metal is removed. Basic metal cutting terminology is presented in Figure 3 [4]. The wedge-shaped cutting tool consists of two surfaces intersecting to form the cutting edge. The chip flows along the surface called the tool face (rake face), and the new machined surface of the workpiece contacts the flank. The undeformed chip thickness refers to the depth of the individual layer of material removed by the action of the tool. The rake angle

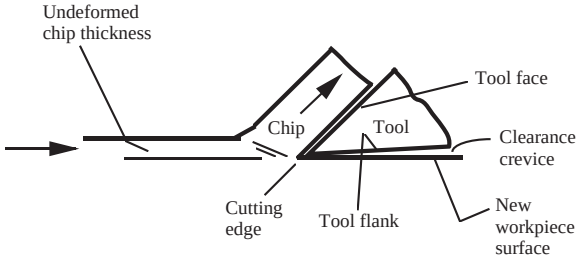

Figure 3: Metal Cutting Terminology.

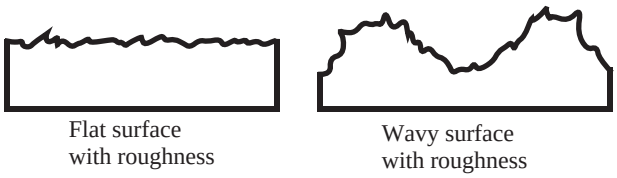

Figure 4: Flat and Wavy Surfaces with Roughness.

is one of the most important variables in metal cutting and is specified in orthogonal cutting by the angle between the tool face and a line perpendicular to the new work surface. Finally, the clearance angle, the angle between the flank and the new workpiece surface, can significantly affect the rate at which the cutting tool wears [4].

Machining Errors

During the cutting process, the cutting edge departs from its ideal position on the workpiece surface, due to errors introduced during the machining process. These departures cause the machined surface profile to be irregular (with waviness and roughness), as opposed to the nominal surface profile. Figure 4 shows an example irregular surface for a better understanding of the concept.

The accuracy of the workpiece produced in metal cutting is largely influenced by departures from the ideal relative movement between the tool and the workpiece. The causes of errors between the tool and workpiece may be divided into geometric and kinematic categories [26]. Geometric deviations are the positional inaccuracies and errors in the shape of the machine components (tables, tool holders, guides, etc.). Kinematic deviations occur during coordinate movements, i.e., functional movements (guideway control, etc.). Production and assembly errors in the elements may cause any of these departures, as well as their elastic deformations due to thermal, dynamic, or static loading conditions [26].

In addition to geometric and kinematic deviations, work accuracy is also influenced by static and dynamic forces deforming the components which are in the force-flux of the machine, such as machine frames, beds, slides, spindles, etc. [26]. Finally, vibrations between the workpiece and the cutting tool will also interfere with the required nominal motions (i.e., feed and cutting movements). These vibrations can be classified as externally-excited or forced vibrations and self-excited vibrations. Externally excited vibrations may result from, for example, interference transmitted from the foundations into the machine system, or from damaged or imperfect machine elements (i.e., unbalanced masses, bearing faults, gear-tooth engagement shocks, etc.). Self-excited vibrations may result from the surface finish waviness induced by the externally-excited vibrations, which lead to excitations after the workpiece has rotated one revolution (in the case of turning). Built-up cutting edge formation and regenerative effects such as chatter also belong to this category [26].

Review of Literature on Metal Cutting Models

Models of machining processes based on machining mechanics are widely reported in the literature [2, 3, 10, 28, 29]. Blackley and Scattergood [2] have used a machining model for diamond turning of brittle materials. They have established a critical depth thickness d_c and a surface damage depth y_c and derived an equation to compute these two parameters from known machining parameters. Zhang and Kapoor [29] have studied the dynamic generation of machined surfaces by developing a model which can correlate the surface finish parameters with the machining conditions, as well as workpiece material characteristics. The machining system example used is a two-degree-of-freedom boring system. The model incorporates a cutting force which includes random excitation, mainly caused by the nonhomogeneous distribution of microhardness in the workpiece material. Wu [28] studies a single degree-of-freedom vibration model of the orthogonal cutting process, where two distinct mechanisms control the cutting process: the chip formation mechanism rising in front of the tool rake face; and the ploughing mechanism occurring at the vicinity of the tool nose region. Both of these mechanisms produce stress fields, and thus forces in equilibrium with these stress fields. In another study by the same author [27], a dynamic force model is developed that accounts for the changes in the plastic state along two deformation fronts in response to the alteration of the cutting configuration: the shear plane (primary deformation zone) and the tool-chip interface (the secondary deformation zone). Forces are derived for this single-degree-of-freedom model in which a flexible tool vibrating normal to the cutting direction is set to remove a layer of workpiece material.

These models generally employ either a one or a two degree-of-freedom vibration model of the cutting tool [2, 10, 27, 28, 29]. In addition, the models in these works account for a few error sources only. In reality, however, there is a greater number of error sources involved in a much more complex machining process. Using the models mentioned in the literature as a basis for comparison, a more comprehensive model is developed in this paper. The model represents the overall machining system in order to incorporate movement and misalignment from all components and parameters, and errors related to system dynamics.

THE TURNING MODEL

Prior to simulating the error profiles of a turned component, an extensive study of the turning machining process is necessary to understand and model the system. The following subsections give a description of the global system, describe the development of an expression for the forces generated at the tool contact point, and finally present the model of the turning system based on bond-graph modeling techniques.

Global System Description

The most widely used machine tool is a lathe, whose main cutting action is rotational [6]. A lathe can perform a variety of turning operations which include external and internal turning, boring, and threading. The current focus of this work is external turning. Turning systems are commonly used for removal of material from components of circular cross section. Despite the benign environment in which a turning system operates, the conditions under which it operates are highly critical. The turning system, like most modern machine tools, is expected to operate with accuracy on the order of microns. This accuracy, combined with the high velocity conditions of the system components, necessitate a highly precise machine [6].

Figure 5 shows an engine lathe in detail. On the left hand side of this figure is the headstock and on the right hand side is the tailstock. Placed between the headstock and the tailstock, are the rotational and the translational sections of the turning system. The upper portion is the rotational section consisting of the spindle, chuck, and the workpiece. The lower translational portion consists of the carriage, which is guided on a feed rod, the cross slide, the tool post, and the cutting tool. The horizontal bed supports the headstock, tailstock, and carriage. The workpiece is usually held at one end by a chuck mounted on the main spindle of the machine and is supported at the other end by a center mounted in the tailstock. The primary motion in the system is the rotation of the workpiece, provided by the movement of a series of gears driving the main spindle. The gears are driven by an electric motor. The main spindle and the gears are mounted in the headstock. The single-point cutting tool is held in a toolpost, mounted on a cross slide, which in turn is mounted on the carriage. The translational movement of the carriage is the feed motion. The carriage is driven along the bed by a lead screw or a rack, pinion gear, and feed rod assembly. The lead screw and feed rod are connected to the main spindle through a gear train. Long workpieces are supported at their end with a center held in the tailstock. The toolpost is mounted on a cross slide, which provides the radial movement. The cross slide is guided in the carriage, which in turn receives support from the ways machined in the bed that ensure rigidity and freedom from vibrations [4, 20]. The typical characteristic ranges for a turning machine using a single-point cutting tool are shown in Table 1.

The turning machine, the tool, and the workpiece form a structural system with complicated dynamic characteristics [6]. The highly precise control under which the turning system has to operate implies that each component and connection between components contribute to the system dynamics. Vibrations occur within the system because of the interaction between the machine tool structure and the cutting tool. These vibrations include free or transient vibrations, forced vibrations, and self-excited vibrations. Free vibrations result from intermittent actions transferred to the turning system. The structure deflects and oscillates in its natural modes of vibration until the damping of the structure reduces the vibrations. Forced vibrations result from periodic forces within the turning system, or are transferred through the machine structure foundations from another system. The turning machine will oscillate at the forcing frequency. Self-excited vibrations also result from a dynamic instability of the process, which will cause the machine to vibrate in one of its natural modes of vibration [6].

During machining, the machine frame is also exposed to dynamic forces, moving the workpiece relative to the cutting tool. The forces exerted by the cutting tool on the workpiece are transmitted to the machine tool table and the turning machine, causing deflection of the machine components. To provide a general idea of the cutting forces, consider an example of turning low carbon steel. When cutting very low carbon steel at a speed of 91.5 m/min (300 ft/min), a feed of 0.25 mm (0.010 in)/rev, and depth of cut of 1.25 mm (0.05 in), the cutting force F_c is measured to be 1400 N (315 lbf), and the feed force is 1310 N (295 lbf), which are quite high [25]. The amount of deflection due to such cutting forces partly depends on the stiffness of the machine components. Components are usually made stiff (rigid) to minimize misalignment, avoid interference, and reduce noise, stress, and wear rates. For example, if a shaft deflects during machining, it can cause shaft and bearing bore misalignment, cause interference between adjacent components, and result in misalignment in attached gears. As a result, the system operating characteristics may be affected, leading to surface irregularities [14].

In addition to dynamic and static behaviors, the machine will also have a thermal behavior. External or internal heat sources may create a temperature field around particular components, which may cause thermal deformation of those components, depending on the temperature field, the geometry of the component, how the component is joined to the machine, and the material of the component. In particular, a relatively high temperature field will be developed around the cutting area about the workpiece surface. For instance, when steel is machined at high speed without the use of a coolant, the chip shows discoloration which indicates a temperature on the order of $250 - 350°$C [25]. Again, thermal deformation will cause the undesired displacement of the tool with respect to the workpiece [6]. The thermal behavior is not specifically addressed in this paper.

It is crucial to limit vibrations and displacements within the turning system in order to inhibit surface irregularities, tool damage, and so on. The precision required at the tolerance scales also necessitates the control of each component's contribution to these vibrations. It is important to understand how and where errors occur and how each component contributes to the system dynamics to prevent or cause system vibrations. The current project aims at including most of the primary error sources and component contributions in the model to simulate a realistic surface profile.

Forces at the Tool Contact Point

The tool contact point is the point where the rotating portion and the translating portion of the system are engaged. When contact occurs, forces are generated in all three directions (x, y, and z), causing cutting to occur. These forces,

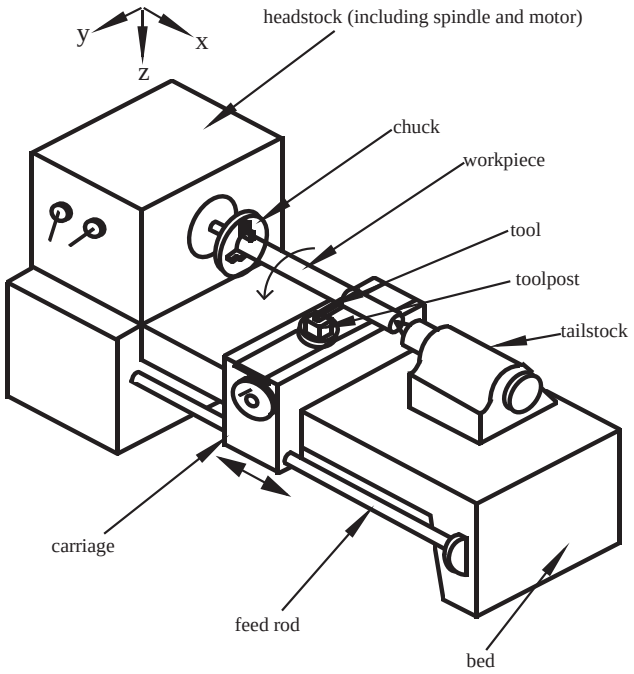

Figure 5: Detailed Engine Lathe.

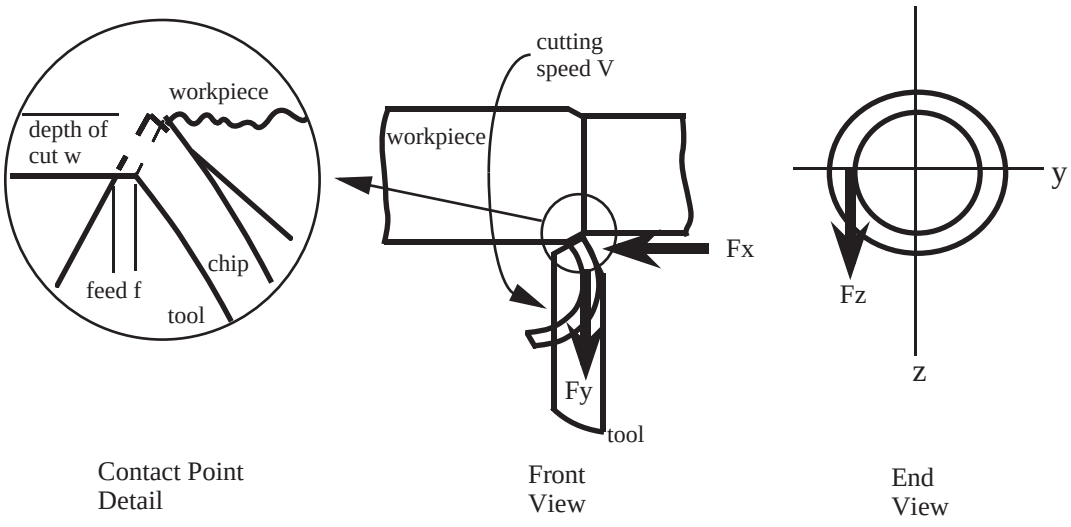

Figure 6: Forces Generated due to Cutting at the Tool Contact Point.

due to their complexity and nonlinearity, are usually derived empirically. In this paper, two empirical force analyses are combined to derive force relationships in three directions, namely, the cutting direction, z, the feed direction, x, and the depth-of-cut direction, y. Some of the factors that must be taken into account when deriving these relationships are the friction generated during cutting in all three directions, as well as some deformation due to the compliance of the contact point. Figure 6 shows the cutting forces generated at the contact point of the tool and the workpiece.

The dynamic cutting force acting on the workpiece is affected by the dynamic variations of depth of cut, cutting velocity, and the rake angle [15]. Marui et al. [15] have derived expressions for the cutting force in the cutting direction F_z and the force in the depth of cut direction F_y. The cutting force is assumed proportional to the depth of cut. The depth of cut during vibration is expressed as:

$$d = d_s - y(t) \tag{1}$$

where d_s is the steady state cutting depth, and $y(t)$ is the variation in the depth of cut. In addition, Grabec [8] has interpreted the dependence of the cutting force F_z and the friction force F_x by a friction coefficient K. Grabec treats a manufacturing system as a simple two dimensional elastic structure in which the cutting force is generated by material flow against the tool. Generalized empirical relationships are used to describe the non-linear dependence of a cutting force on chip velocity and thickness.

Combining these ideas from Marui et al. and Grabec and linearizing, we derive the following expressions for the cutting forces in the x, y, and z directions:

$$\begin{aligned} F_x &= A_1 x(t) + B_1 y(t) + C_1 \dot{x}(t) + D_1 \dot{y}(t) \\ &+ E_1 \dot{z}(t) + F_1 \qquad (2) \\ F_y &= A_2 x(t) + B_2 y(t) + D_2 \dot{y}(t) + E_2 \dot{z}(t) + F_2 \qquad (3) \\ F_z &= A_3 x(t) + B_3 y(t) + D_3 \dot{y}(t) + E_3 \dot{z}(t) + F_3 \qquad (4) \end{aligned}$$

where x is the feed motion direction, y is the depth of cut direction, and z is the direction tangent to the rotational motion of the workpiece.

These relationships, as well as the values for the constants, are presented in Appendix A. The nature of these force relationships dictates what characteristics the model should possess. For instance, the expressions dictate a dependence on displacement and velocity variables; the constants accompanying these variables represent stiffness and damping, respectively.

Bond Graph Representation

A model is a simple and abstract construct used to predict system behavior [9]. System modeling is typically defined by two goals [5]. The first goal aims at representing all physically realizable systems. The second goal requires that all possible system models correspond to realizable physical systems. A modeling technique called bond graph modeling is, in general, capable of achieving both goals better than other modeling techniques [5].

Bond graphs constitute a systematic modeling technique, have been increasingly used to model complex dynamic systems [24, 23], and are suitable to model machining processes. Bond graphs, based on energy and information flow, provide a uniform notation to construct system models for all types of physical systems, allowing one to study the structure of a system model. A bond graph simply consists of subsystems connected by ports represented by lines which correspond to power bonds [9]. Energy leaving one subsystem is instantaneously received by the next subsystem. The models are translated into differential equations or computer simulation schemes by using standard techniques. Bond graph equations use state variables such as q and p (displacement and momentum), which together represent the energy state of a system [19]. The reader is referred to Karnopp et al. [9] for more detail.

As a brief review, a bond graph, along with the constitutive relationships and the connecting equations at the junctions, provides a set of state equations which is a set of coupled first order differential equations. The variables in these state equations are called state variables and are determined by stiffness and inertia elements that are independent after causality has been assigned. Common flow in the system is designated by a 1-junction, and common effort by a 0-junction. The C, I, and B elements are the compliance, inertia, and internal damping respectively. The energy storing elements (C and I) and the dissipative element (B) each have constitutive relations that are used to expand the connecting equations.

Based on the physics of turning machines, a bond graph model is developed for the turning system, as shown in Figure 7. The upper portion of the bond graph model represents the rotational components. Each rotating component, namely the spindle, the chuck, and the workpiece, is assumed to have a rotary inertia, shown as J, a torsional compliance C, and an internal damping B. The spindle angular velocity is transformed to the translational feed velocity by means of a set of gears. The translational components are assumed to move and/or oscillate in three directions. In the x direction (feed motion), a percentage of the transformed feed velocity translates the linear inertia element, denoted as I, and the remainder is absorbed by the internal damping and compliance of the translational components. In the y direction (depth-of-cut direction), and the z direction (cutting direction), the translational components have no prescribed motion, exhibiting oscillatory behavior only. In these two directions, the inertia, damping, and compliance elements move at the same velocity. At the tool contact point, the forces generated during cutting result in two multiport fields. The two multiport fields are shown on the bond graph model as one three-port dissipation field, and one two-port contact compliance field in the x and y directions. These multiport fields help in describing the coupling between motions in the three directions. The variables of interest for simulation purposes are the x, y, and z motions at the tool-workpiece contact point, since these motions directly represent the surface irregularities. Simulation results are presented in the following sections. The state equations developed for the entire

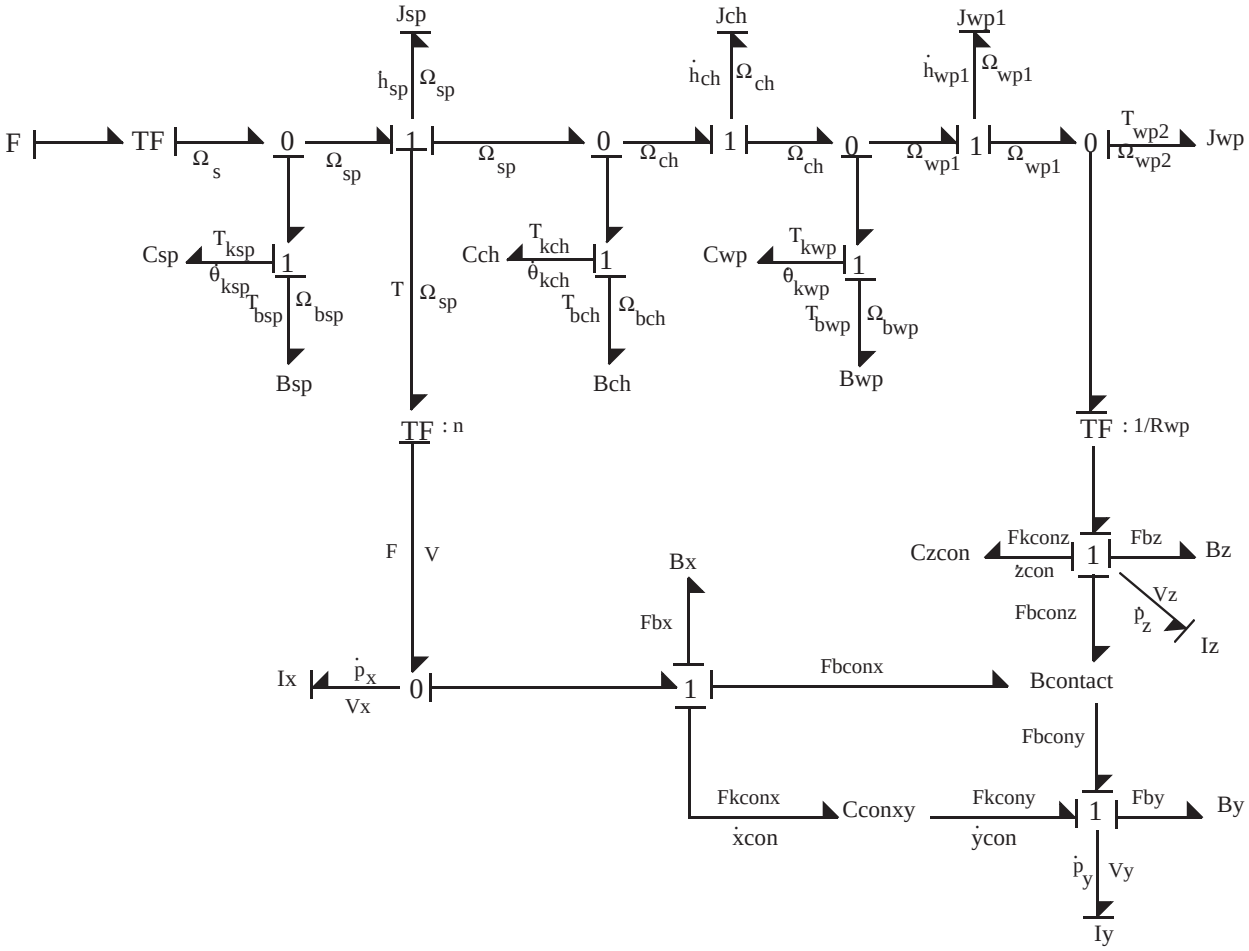

Figure 7: Bond Graph Model of the Engine Lathe Turning System.

Table 1: Typical Parameters and Characteristics for Turning Lathes.

Characteristics	*TypicalRanges*
Rotational speed	0.3 to 27 rad/sec (20 to 1600 rpm)
Feed	0.05 to 2.5 mm (0.002 to 0.1 in)
Power	4 kW (5 hp)
Overall Efficiency	70 %
Max Machining Accuracy	0.013 mm (0.0005 in)
Max Workpiece Length	760 mm (30 in)
Max Workpiece Diameter	360 mm (14 in)

system are presented in Appendix B.

SIMULATION

The model simulation must accurately describe the turning system based on the system physics. The preliminary model incorporates most of the dynamics of the lathe components. However, the model does not include the external friction effects, the thermal effects, or the random cutting force effects. Nonetheless, the model is expected to provide results that closely compare to the experimental surface profiles, which will be obtained later in the project, and also follow the shaping simulation results obtained by Srinivasan and Wood [21]. These surfaces are also expected to result in comparable fractal dimensions. Changes in design and cutting parameters are expected to result in a change in fractal dimension.

The following subsections provide a discussion and interpretation of the obtained results based on sensitivity and fractal analyses.

Results and Interpretation

The vibrations in the x, y, and z directions cause a resultant error in the tool position relative to the workpiece, resulting in circularity and/or diametric (size) errors in the workpiece. This phenomenon is illustrated in Figure 8, which depicts two plots of the workpiece radius as a function of the position along the circumference for one revolution of the workpiece. The two cases illustrated correspond to low spindle angular speed, and high tool and toolpost stiffness. The complete set of different cases are presented as part of the sensitivity and fractal analyses below.

The sample profiles shown in Figure 8 represent the error profiles computed based on the model. The profile error is calculated both in terms of an "error zone" and a "fractal dimension". The former parameter is obtained from the extrema of the radial distances, and the latter is estimated using the algorithm developed in reference [21]. This algorithm is briefly described below.

The irregular profile variations resulting from a cutting process are analyzed using a box-counting method. The box-counting method is analogous to the use of a dial indicator to traverse the surface profile of a machined part where the dial indicator probe movement measures the error of the profile. The profile is covered with boxes of different sizes, corresponding to different probe sizes. The algorithm counts one box for each interval along the surface profile in the horizontal direction and a fractional number of boxes for the height variation in the vertical direction. The fractal dimension is derived from the power-law relationship between the total number of boxes and the box size [21].

Using the box-counting algorithm and the state-space simulation results, the bond-graph model is used to generate profiles for a typical general-purpose lathe, and the maximum error and the fractal dimension are calculated for each profile. In addition, a sensitivity analysis of the model over the various dynamic and process parameters is carried out. The results are presented in Table 2.

Figure 8: Surface Profile Plots.

The main purpose of the fractal analysis of the turned surface profiles is to prove the validity of the fractal hypothesis in showing the interaction between cutting and design parameters. In particular, simulations followed by an error analysis are carried out for the following cases: varying mass, varying internal damping, varying stiffness, and finally, varying speeds in the turning system. The mass, damping, and stiffness values are the values calculated for the tool and the toolpost, corresponding to the main contributors to the system dynamics. A study of the various results indicates certain specific trends. Both the fractal dimension and the error zone decrease with an increase in the design parameters, notably the internal damping, the stiffness, and the mass. For the cutting parameter, an increase in the spindle rotational speed results in a decrease in the fractal dimension and an increase in the error zone. This trend is indicative of a frequency-amplitude relationship of the error profile. A decreasing fractal dimension and increasing error zone represent a profile structure with increasing amplitude and decreasing frequency. In general, a simultaneous consideration of the fractal dimension and the error zone is desired to assess the influence of the surface variation on the product function. However, for the design parameters, considering one of the error indicators is sufficient, as both indicators exhibit similar trends. The table shows the details of the sensitivity analysis.

In addition to these results, coupling effects can also be

Table 2: Fractal and Sensitivity Analysis Results.

M	Bx	By	Bz	Kx	Ky	Kz	$SPEED$	Δh_{max}	D_f
(kg)	(kg/s)	(kg/s)	(kg/s)	(kg/s^2)	(kg/s^2)	(kg/s^2)	(rad/s)	(mm)	
3.5	722.	632.	1424.	5.8e8	7.e6	6.e8	25.	0.109	1.00267
							79.6	0.115	1.00072
							125.	0.117	1.00037
10.0							25.0	0.0983	1.0021
40.0				5.8e8	7.e6	6.e8	25.	0.0982	1.000672
3.5				5.8e9	7.e7	6.e9	25.	0.00813	1.000188
10.0				5.8e9	7.e7	6.e9	25.	0.00899	1.000673
3.5	500.0	500.0	500.0	5.8e8	7.e6	6.e8	25.	0.11233	1.004880
10.0								0.0994	1.00329
3.5				5.8e9	7.e6	6.e8		0.00838	1.000251

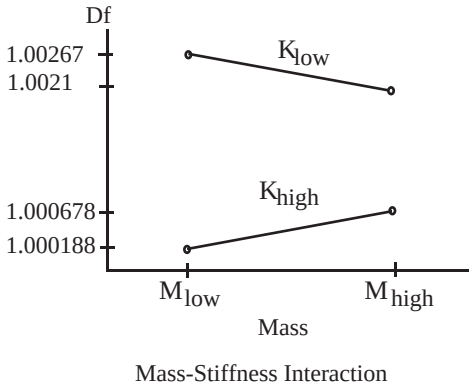

Figure 9: Example of an Interaction Plot.

deduced from the sensitivity and fractal analyses.

Interaction implies coupling between the parameters. In general, interactions are indicated graphically by nonparallel plots of the desired response, i.e., the fractal dimension [16]. The degree of interaction is dependent on the slope of the response curves. If the responses are parallel, there exists no interaction. As the difference in slope increases, the interaction is more significant. The interaction plots show a significant interaction between the mass and the stiffness of the system, less interaction between the mass and the damping, and very little interaction between the damping and the stiffness of the system. Interaction plots are produced by maintaining a low value of one parameter, while varying the other parameter, and maintaining a high value of the same parameter while varying the parameters by the same amount. One of these plots is presented in Figure 9 as an illustrative example for the first case discussed above.

Overall, the results are consistent with the initial findings of the shaping process reported in [21], and compare favorably to empirical data from turning machines. Specifically, the surfaces generated by the lathe turning process based on the model developed in this research are fractal. The model presented in this paper is more comprehensive than other models found in the literature, including all the major structural and dynamic features of the lathe. The agreement of the results with those of the simpler shaping model validates the use of fractal measures for machining mechanics. In addition, from the sensitivity analysis, the expected maximum accuracy of a turning lathe, on the order of $0.01mm$, is obtained in most cases. This is consistent with the empirical results from machining handbooks. The potential for the development of a "complete" model for the turning process is a promising beginning to understanding and using manufacturing variations in mechanical design.

FUTURE WORK

As part of future work, two primary tasks will be completed: experimentation and inclusion of more dynamic effects. The outputs of the modeled profiles need to be compared to actual surface profiles. The physical surface profiles of turned parts will be measured using a fiber optic device or dial gage arrangement. The comparison of the modeled surface profile and the actual surface profile will show the accuracy of the model. As a consequence of this comparison, the surface model will be improved to include a larger number of error sources, including modifications to the original assumptions made for the model. In addition, elements that were neglected in this work, such as resistive elements caused by friction between components, bearing friction, and electric motor resistance, as well as surface variations caused by the thermal expansion effects at the tool-workpiece contact point, and the effects of random cutting forces will be

incorporated in the model for completeness.

The fractal analysis of both the experimental surface and the improved modeled surface will eventually provide a tolerance value for the machining process and parameters in question. To complete the fractal-based tolerancing hypothesis followed in this work, the procedure described in this paper will be applied to other machining processes as well.

CONCLUSIONS

In this paper, simulation results of a surface profile analysis are presented. As a foundation for this investigation, a bond graph model of the turning process is developed, based on machining mechanics and system physics. This model represents a more comprehensive approach than other machining models that appear in the literature. Tool point forces in each degree of freedom are coalesced into a general three-dimensional relation. The model also incorporates the dynamic and static behaviors of each component of the turning system, which affect the surface variation of a machined part. These simulated surfaces are analyzed using a fractal-based box counting algorithm, and show favorable results when compared to previous research on the fractal characteristics of machined surfaces. The bond graph model developed in this paper will provide a sound foundation for studying the precision of surface profiles generated by a turning process, and provide a platform for developing fractal-based tolerance measures of turned parts. If such tolerance measures are found to characterize the precision of machines, the designer will gain a means of choosing design and cutting parameters in advance, based on the predicted surface structure.

ACKNOWLEDGEMENTS

This material is based upon work supported, in part, by The National Science Foundation, Grant No. DDM-9111372, an NSF REU supplement grant; and an NSF Young Investigator Award. Any opinions, findings, conclusions or recommendations expressed in this publication are those of the authors and do not necessarily reflect the views of the sponsors.

References

[1] O. Bjorke. *Computer-Aided Tolerancing.* John Wiley and Sons., New York, 1989.

[2] W.S. Blackley and R.O. Scattergood. Ductile-regime machining model for diamond turning of brittle materials. *Precision Engineering*, 13:95–103, April 1991.

[3] P. Blake, T. Bifano, and R.O. Scattergood. Precision engineering of ceramic materials. *Ceramic Bulletin*, 67:1038–1044, June 1988.

[4] G. Boothroyd and W.A. Knight. *Fundamentals of Machining and Machine Tools.* Marcel Dekker Inc., New York, 1989.

[5] I.J. Busch-Vishniac and H.M. Paynter. Bond graph models of sound and vibration systems. *Journal of Acoustics*, 85:1750–1756, April 1989.

[6] G. Chryssolouris. *Manufacturing Systems: Theory and Practice.* Springer-Verlag, New York, 1992.

[7] E.L. Church. Fractal surface finishing. *Applied Optics*, 27(8):1518, 1988.

[8] I. Grabec. Chaotic dynamics of the cutting process. *International Journal of Machine Tools Manufacturing*, 28:19–32, May 1988.

[9] D.C. Karnopp, D.L. Margolis, and R.C. Rosenberg. *System Dynamics: A Unified Approach.* John Wiley and Sons, 1990.

[10] S.J. Lacey. Vibration monitoring of the internal centreless grinding process, part 1: Mathematical models. *Journal of Engineering Manufacture*, 204(B2):119–142, 1990.

[11] A. Majumdar and B. Bhushnan. Role of fractal geometry in roughness characterization and contact mechanics of surfaces. *Journal of Tribology*, 112:205, April 1990.

[12] A. Majumdar and C.L. Tien. Fractal characterization and simulation of rough surfaces. *Wear*, 136(2):313–327, March 1990.

[13] B.B. Mandelbrot. *The Fractal Geometry of Nature.* Freeman, W.H, and Co.,, San Fransisco, 2nd edition, 1983.

[14] K. M. Marshek. *Design of Machine and Structural Parts.* John Wiley and Sons, Canada, 1987.

[15] E. Marui, S. Kato, M. Hashimoto, and T. Yamada. The mechanism of chatter vibration in a spindle-workpiece system: part- characteristics of dynamic cutting force and vibration energy. *Journal of Engineering for Industry*, 110:242–247, August 1988.

[16] R.L. Mason, R.F. Gunst, and J.L. Hess. *Statistical Design and Analysis of Experiments: with applications to engineering and science.* John Wiley and Sons, New York, 1989.

[17] H.-O. Peitgen and D. Saupe. *The Science of Fractal Images.* Springer-Verlag, New York, 1988.

[18] A.A. Requicha. Toward a theory of geometric tolerancing. *The International Journal of Robotics Research*, 2(4):45–60, 1983.

[19] R.C. Rosenberg and D.C. Karnopp. *Introduction to Physical System Dynamics.* McGraw-Hill Inc., 1987.

[20] J.A. Schey. *Introduction to Manufacturing Processes.* McGraw-Hill Inc., 1987.

[21] R.S. Srinivasan and K.L. Wood. A computational investigation into the structure of form and size errors based on machining mechanics. In *ASME Design Automation Conference*, pages 161–171, September 1992.

[22] R.S. Srinivasan and K.L. Wood. Fractal-based representations in design and manufacturing. In *NSF Design and Manufacturing Systems Conference*, pages 407–411, 1992.

[23] J.L. Stein, C. Calvin, G. Clever, and C.-H. Wang. Evaluation of DC servo machine tool feed drives as force sensors. *Journal of Dynamic Systems, Measurement, and Control*, 108:279, December 1986.

[24] J.L. Stein and C.-H. Wang. Analysis of power monitoring on AC induction drive systems. *Journal of Dynamic Systems, Measurement, and Control*, 112:235, June 1990.

[25] E.M. Trent. *Metal Cutting*. Butterworths, London, 1984.

[26] M. Weck. *Handbook of Machine Tools, Volume 4: Metrological Analysis and Performance Tests*. John Wiley and Sons, Dusseldorf, 1984.

[27] D.W. Wu. Comprehensive dynamic cutting force model and its application to wave-removing processes. *Journal of Engineering for Industry*, 110:153–161, May 1988.

[28] D.W. Wu. A new approach of formulating the transfer function for dynamic cutting processes. *Journal of Engineering for Industry*, 111:37–47, February 1989.

[29] G.M. Zhang and S.G. Kapoor. Dynamic generation of machined surfaces, parts 1 and 2. *Journal of Engineering for Industry*, 113:137–153, May 1991.

[30] H.C. Zhang and M.E. Huq. Tolerancing techniques: the state-of-the-art. *International Journal of Production Research*, 30:2111–2135, January 1992.

A DERIVATION OF FORCES AT TOOL CONTACT POINT

The following is a brief description of the three-dimensional force expressions. Conditions : orthogonal cutting with tool vibrations; d_s= steady state depth of cut; cutting force proportional to variations in depth of cut, cutting velocity, and rake angle; neglect second order terms for simplicity assume y, $\dot{y}(t)$, and $\dot{z}(t)$ are small.

Based on the expressions for the forces in the two directions y and z in Marui et al. [15], and the dependence of the force in the z direction (cutting direction) and the force in the x direction (feed direction) by a nonlinear friction coefficient developed by Grabec [8], going through a complicated set of mathematical manipulations, the following resulting expressions are obtained for F_x, F_y, F_z:

$F_x = A_1 x(t) + B_1 y(t) + C_1 \dot{x}(t) + D_1 \dot{y}(t) + E_1 \dot{z}(t) + F_1$

Table 3: Empirical Constants

d_s	V_i	h_i	a_{yv}	a_{cv}	a_{yr}
m	m/s	m/rev	Ns/m^3	Ns/m^3	N/m^2
1.016e-3	1.016	1.78e-4	0.64e9	2.75e6	1.75e9
a_{cr}	K_{y_0}	K_{c_0}	$C1$	$C2$	$C3$
N/m^2	J/m^3	J/m^3			
1.11e9	1.36e9	3.75e9	0.3	0.7	1.5
$C4$	r_0	h_0	V_0	k_0	–
		m/rev	m/s		
1.2	2.2	2.5e-4	6.6	0.36	-

Table 4: Calculated Constants

A_1	B_1	C_1	D_1	E_1	F_1
kg/s^2	kg/s^2	kg/s	kg/s	kg/s	kgm/s^2
1.83e6	5.7e5	152.23	25.72	486.93	578.76
A_2	B_2	C_2	D_2	E_2	F_2
kg/s^2	kg/s^2	kg/s	kg/s	kg/s	kgm/s^2
345.44	-3.4e5	0.0	67.35	1.6e5	345.44
A_3	B_3	C_3	D_3	E_3	F_3
kg/s^2	kg/s^2	kg/s	kg/s	kg/s	kgm/s^2
952.5	9.4e5	0.0	42.33	687.5	952.5

$F_y = A_2 x(t) + B_2 y(t) + D_2 \dot{y}(t) + E_2 \dot{z}(t) + F_2$
$F_z = A_3 x(t) + B_3 y(t) + D_3 \dot{y}(t) + E_3 \dot{z}(t) + F_3$
Or, expressed in another form:
$F_{Bconx} = B_{11} V_{bconx} + B_{12} V_{bcony} + B_{13} V_{bconz}$
$F_{Bcony} = B_{22} V_{bcony} + B_{23} V_{bconz}$
$F_{Bconz} = B_{32} V_{bcony} + B_{33} V_{bconz}$
$F_{Kconx} = A_{11} X_{kcon} + A_{12} Y_{kcon} + C_1$
$F_{Kcony} = A_{21} X_{kcon} + A_{22} Y_{kcon} + C_2$
$F_{Kconz} = A_{31} X_{kcon} + A_{32} Y_{kcon} + C_3$
The values for these constants are presented in Table 3 and Table 4.

B THE STATE EQUATIONS

The following appendix presents the state equations derived from the bond graph model. The set of first order differential equations along with the constants, provide the necessary input to perform simulations. The first transformer modulus, n, is related to the feed of the system, and the

Table 5: Constants Calculated for the State Equations.

n	R_{work}	$K_{spindle}$	$J_{spindle}$	$B_{spindle}$
	m	kgm/s^2	kgm^2	kg/s
2.83e-5	1.825e-2	7586.7	1.e-4	3.1e-3
K_{chuck}	J_{chuck}	B_{chuck}	K_{work}	B_{work}
kgm/s^2	kgm^2	kg/s	kgm/s^2	kg/s
5.9e7	0.078	8.55	8.17e4	0.029
J_{work1}	J_{work2}	M	B_x	B_y
kgm^2	kgm^2	kg	kg/s	kg/s
3.e-4	2.e-4	3.5	722	632.
B_z	K_x	K_y	K_z	
kg/s	kg/s^2	kg/s^2	kg/s^2	
1424.	5.85e8	7.18e6	6.06e8	

second transformer modulus, R_{work}, is related to the depth of cut of the system. M is the mass, J is the rotary inertia, K is the stiffness, B is the internal material damping, H is the angular momentum, P is the linear momentum, Θ is the torsional oscillations, Ω is the angular speed, and X, Y, and Z are the translational oscillations in three directions, corresponding to the desired error profile. The constants used in the state equations are listed in Table 5.

$$\dot{\Theta}_{spindle} = \Omega_{spindle} - \frac{1}{J_{spindle}} H_{spindle} \quad (5)$$

$$\begin{aligned}\dot{H}_{spindle} &= K_{spindle}\Theta_{spindle} - K_{chuck}\Theta_{chuck} \\ &+ B_{spindle}\Omega_s + \frac{B_{chuck}}{J_{chuck}} H_{chuck} \\ &- \frac{B_{spindle} + B_{chuck} + n^2(B_x + C_1)}{J_{sp}} H_{spindle} \\ &+ \frac{n}{M}(B_x + C_1)P_x - \frac{D_1 n}{M} P_y \\ &- \frac{E_1 n}{M} P_z - K_x n X_{contact} \\ &+ B_1 n Y_{contact} - F_1 n \end{aligned} \quad (6)$$

$$\dot{\Theta}_{chuck} = \frac{1}{J_{spindle}} H_{spindle} - \frac{1}{J_{chuck}} H_{chuck} \quad (7)$$

$$\begin{aligned}\dot{H}_{chuck} &= K_{chuck}\Theta_{chuck} + \frac{B_{chuck}}{J_{spindle}} H_{spindle} \\ &- \frac{B_{chuck} + B_{work}}{J_{chuck}} H_{chuck} - K_{work}\Theta_{work} \\ &+ \frac{B_{work}}{J_{work1}} H_{work1} \end{aligned} \quad (8)$$

$$\dot{\Theta}_{work} = \frac{1}{J_{chuck}} H_{chuck} - \frac{1}{J_{work}} H_{work} \quad (9)$$

$$\begin{aligned}\dot{H}_{work_1} &= L_1 L_3 K_{work}\Theta_{work} + \frac{L_1 L_3 B_{work}}{J_{chuck}} H_{chuck} \\ &- \frac{L_1 L_3 B_{work}}{J_{work1}} H_{work1} \\ &- L_7(B_z + E_3)P_z - L_7 D_3 P_y \\ &+ A_3 L_6 X_{contact} + B_3 L_6 Y_{contact} \\ &- L_6 K_z Z_{contact} - F_3 L_6 \end{aligned} \quad (10)$$

$$\begin{aligned}\dot{P}_z &= L_5 K_{work}\Theta_{work} + \frac{L_5 B_{work}}{J_{chuck}} H_{chuck} \\ &- \frac{L_5 B_{work}}{J_{work1}} H_{work1} - \frac{(L_4 + L_2)(B_z + E_3)}{M} P_z \\ &- \frac{D_3(L_4 + L_2)}{M} P_y + A_3(L_4 + L_2)X_{contact} \\ &+ B_3(L_4 + L_2)Y_{contact} - (L_4 + L_2)K_z Z_{contact} \\ &- A_3(L_4 + L_2) \end{aligned} \quad (11)$$

$$\begin{aligned}\dot{P}_x &= \frac{(B_x + C_1)n}{J_{spindle}} H_{spindle} - \frac{(B_x + C_1)}{M} P_x \\ &+ \frac{D_1}{M} P_y + \frac{E_1}{M} P_z \\ &+ K_x X_{contact} - B_1 Y_{contact} + F_1 \end{aligned} \quad (12)$$

$$\dot{X}_{contact} = \frac{n}{J_{spindle}} H_{spindle} - \frac{1}{M} P_x \quad (13)$$

$$\begin{aligned}\dot{P}_y &= \frac{(D_2 - B_y)}{M} P_y + \frac{E_2}{M} P_z \\ &- A_2 X_{contact} - K_y Y_{contact} + F_2 \end{aligned} \quad (14)$$

$$\dot{Y}_{contact} = \frac{1}{M} P_y \quad (15)$$

$$\dot{Z}_{contact} = \frac{1}{M} P_z \quad (16)$$

where

$L_1 = \frac{1}{1 + \frac{J_{work2}}{J_{work1}}}$

$L_2 = \frac{1}{1 + \frac{J_{work2}}{MR^2_{work}}}$

$L_3 = \frac{1}{1 - \frac{L_1 L_2 J^2_{work2}}{M J_{work1} R^2_{work}}}$

$L_4 = \frac{L_1 L_3 L_2^2 J^2_{work2}}{M J_{work1} R^2_{work}}$

$L_5 = \frac{L_1 L_2 L_3 J_{work2}}{J_{work1} R_{work}}$

$L_6 = \frac{L_1 L_2 L_3 J_{work2}}{M R_{work}}$

$L_7 = \frac{L_1 L_2 L_3 J_{work2}}{R_{work} M^2}$